ESA Climate Change Initiative Plus - Soil Moisture

Algorithm Theoretical Basis Document (ATBD) – Medium Resolution (MR)

D2.8 Version 1.0

Supporting Product Version v09.2

27/11/2025

Prepared by

Earth Observation Data Centre for Water Resources Monitoring (EODC) GmbH

in cooperation with

TU Wien, Transmissivity, CESBIO and UKCEH

This document forms the deliverable D2.8 Algorithm Theoretical Basis Document (ATBD) – Medium Resolution (MR), Version 1.0, and was compiled for Phase 3 of the ESA Climate Change Initiative Plus Soil Moisture Project (CCN 4 to ESRIN Contract No: 4000126684/19/I-NB). For more information on the CCI programme of the European Space Agency (ESA) see https://climate.esa.int/.

Number of pages: 23 (including cover, preface and references).

Authors:		D. D.Kovács, C. Moldenhauer, W. Preimesberger, J. Lems, W. Dorigo
Circulation (Internal):		Project consortium and science partners
External:		ESA

Issue		Date	Details	Editor
0.1		03/10/2025	Created Based on approved ATBD v9.0	DDK, CM, WP, JL
0.2		06/10/2025	Review	WD
0.3		14/10/2025	Finalised document	DDK, CM
0.4		29/10/2025	Reviewed, updated document metadata, updates total pages, updated headers, resolved all comments, removed unrequired bookmark inserts. To ESA for review	R. Kidd
0.5		27/11/2025	Incorporate ESA review, update appendix, add known limitations	CM, DDK

For any clarifications please contact Wouter Dorigo (wouter.dorigo@geo.tuwien.ac.at).

Project Partners	
Prime Contractor, Project Management	**EODC**, Earth Observation Data Centre for Water Resources Monitoring (Austria)
Earth Observation Partners	**TU Wien**, Vienna University of Technology (Austria)
	TMS, Transmissivity BV (The Netherlands)
	CESBIO, CESBIO (France)
Climate Research Partner	**UKCEH**, UK Center for Ecology and Hydrology (United Kingdom)

Table of Content

List of Tables

List of Figures

Definitions, acronyms and abbreviations

AMSR2	Advanced Microwave Scanning Radiometer 2
AMSR-E	Advanced Microwave Scanning Radiometer-Earth Observing System
ASCAT	Advanced Scatterometer (MetOp)
ATBD	Algorithm Theoretical Basis Document
BT	Brightness Temperature
CCI	Climate Change Initiative
ECMWF	European Centre for Medium-Range Weather Forecasts
ERS	European Remote Sensing Satellite
ERA5	ECMWF Reanalysis v5
ESA	European Space Agency
GLDAS	Global Land Data Assimilation System
GMI	Global Precipitation Measurement Microwave Imager
H-SAF	Satellite Application Facility on Support to Operational Hydrology and Water Management
ISMN	International Soil Moisture Network
LPRM	Land Parameter Retrieval model
MR	Medium Resolution
MPDI	Microwave Polarization Difference Index
NetCDF	Network Common Data Form
RFI	Radio Frequency Interference
SM	Soil Moisture
SMAP	Soil Moisture Active Passive satellite mission
SMMR	Scanning Multichannel Microwave Radiometer
SMOS	Soil Moisture and Ocean Salinity
SSM/I	Special Sensor Microwave Imager
TCA	Triple Collocation Analysis
TMI	TRMM Microwave Imager
VOD	Vegetation Optical Depth
WindSat	WindSat Spaceborne Polarimetric Microwave Radiometer

1 Introduction

The document is an Appendix to the Algorithm Theoretical Basis Document (ATBD) v9.0 (Dorigo W. s.-F., 2024) of the ESA CCI SM production framework. The previous ATBD for the ESA CCI Soil Moisture production system described the algorithms underlying the generation of soil moisture products, outlining their development within the CCI framework. It provided an overview of the problem and the production system, detailed the retrieval of soil moisture from active microwave sensors, and explained the VUA-NASA LPRM approach for passive sensors. In addition, it documented the methodology for merging active and passive products to produce consistent long-term soil moisture datasets.
This document highlights changes with respect to the processing described in the previous document, for unchanged processing behaviour, we refer to the previous ATBD. Changes in the processing include a change in resampling resolution, minor differences in the collocation procedure and scaling, and thresholds for VOD masking were adapted.

1.1 Purpose of the document

The ESA CCI SM MEDIUM RESOLUTION product is distributed as a stand-alone science product as part of the "ESA CCI Soil Moisture Science data records" community at TU Wien research data at https://doi.org/10.48436/exxcr-tww10 (DOI resolves to the latest published version). The "operational" ACTIVE, PASSIVE, and COMBINED products – along with all previous version – are hosted at https://catalogue.ceda.ac.uk.

The document provides the following:

- The context of providing a Medium Resolution product as part of the ESA CCI satellite SM data suite
- A summary of input data sets and their coverage
- An overview of the resampling and retrieval algorithm with references to the related literature.
- A summary of the output product

1.2 Targeted audience

This document targets the following audience

- Users of the ESA CCI SM Medium resolution surface soil moisture product
- System Engineers for the ESA CCI SM product
- Other CCI ECV projects

2 Background

The main ESA CCI SM product provides surface soil moisture (SSM) observations with a daily sampling on a global 0.25° x 0.25° grid. The new medium resolution (MR) science product is conceptually similar to the main product, however at a spatial resolution of 0.1° degrees. The MR product delivers COMBINED SSM data globally for the time period 2002-2024. The production of the MR product follows the same methodology as the main CCI product, with changes introduced to account for the higher resolution as described in Section 4.1. See **Error! Reference source not found.** for an overview of changes with respect to ESA CCI v9.2.

An important goal of the MR product is an improved capturing of mesoscale soil moisture patterns. Variability in soil moisture at this scale plays a key role in triggering convective storms through land–atmosphere interactions (Chug, 2023). In particular, SM contrasts at scales of 10–40 km have been shown to strongly influence the initiation of mesoscale convective systems (MCSs) in the Sahel (Taylor, 2011), where these storm systems contribute most of the annual rainfall (Mathon, 2002). SM products at 0.25° resolution have proven too coarse to resolve the land surface features linked to such initiations (Taylor, 2011).

3 Input data and coverage

The MR product is based on a selection of active (a) and passive (p) sensors included in the main CCI product:

- ASCAT-A (a), 2007-01-01 until 2021-11-24
- ASCAT-B (a), 2013-06-01 until 2024-12-31
- ASCAT-C (a), 2019-04-01 until 2024-12-31
- AMSR-E (p), 2002-06-19 until 2011-10-04
- AMSR-2 (p), 2012-07-03 until 2024-12-31
- GMI (p), 2014-03-04 until 2024-12-31
- FengYun-B (p), 2010-11-18 until 2019-08-19
- FengYun-C (p), 2013-09-29 until 2020-01-01-06
- FengYun-D (p), 2019-01-01 until 2024-12-31
- SMOS (p), 2010-01-13 until 2024-12-31
- SMAP (p), 2015-04-09 until 2024-12-31

The following sensors are **not** included: SMMR and ERS are omitted due to their coarse native resolution (>50 km), SSM/I and SSMIS are omitted because of their frequency, TMI only covers regions between ±35° latitudes and WindSat had no reference data for evaluation. The temporal coverage ranges from 2002 19th June to 2024 31st December, with daily resolution.

Table 1: Frequencies of sensors used in the CCI MR product. Bold underscore: frequencies used to retrieve soil moisture. (*) For FY and GMI X band = 10.65 GHz.

Sensor	L	C		X	Ku	K	Ka
	1.4 GHz	5.3 GHz	6.9 GHz	7.3 GHz	10.7 GHz	18.7 GHz	23.8 GHz	36.5 GHz
ASCAT		X						
AMSR2			X	X	X	X	X	X
AMSR-E			X		X	X	X	X
FY-3B					X*	X	X	X
FY-3C					X*	X	X	X
FY-3D					X*	X	X	X
GMI					X*	X	X	X
SMAP	X							
SMOS	X							

4 Algorithm

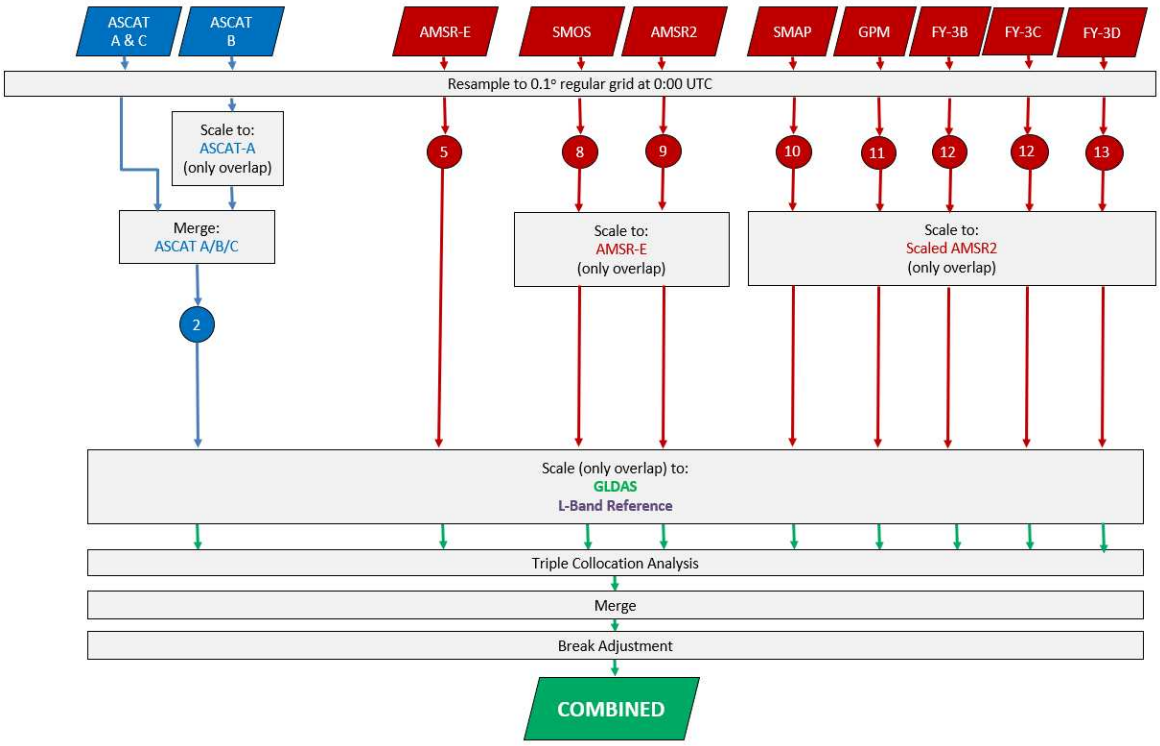

Figure 1: Overview of the processing steps in the ESA CCI SM MR product generation

4.1 Changes to the ESA CCI merging algorithm

The production of the MR product involved most of the steps as used in v9.2 COMBINED. This section is dedicated to describing the changes and adjustments in the merging procedure that were introduced to account for the 0.1° resolution. The main merging steps are summarized in **Error! Reference source not found.**, while full details can be found in the v9.2 ATBD (Dorigo W. s.-F., 2024).

Table 2: Similarities and differences in the CCI merging process, with section numbers referring to the v9.2 ATBD

Section in v9.2 ATBD	Step	ESA CCI v9.2	MR v1.0
7.2.1	**Spatial resampling – (VOD mask)**	• 0.25° grid • Custom VOD thresholds for each sensor-frequency	• 0.1° grid • VOD>0.85 filtered for non L-band sensors, 0.8 for L-band sensors
7.2.1	**Temporal resampling**	Sample nearest valid observation to 0:00 UTC	Same as v9.2
7.2.1	**Cross-flagging – (Frozen soil mask)**	Any sensor needs to detect frozen soil to flag pixel	Majority of sensors need to detect frozen soil to flag pixel
6.2.6	**RFI**	Standard error Method (de Nijs, 2015)	Same as v9.2
7.2.2	**Merging ASCAT**	Arithmetic mean of sensors	Same as v9.2
7.2.3	**Scaling**	Seasonal rescaling approach	Cumulative distribution function matching
7.2.4	**Error characterization**	Triple collocation analysis	Same as v9.2
7.2.5	**Error Gap-Filling**	Polynomial regression between VOD and error estimates	Same as v9.2
7.2.6	**Merging**	Weighted average accounting for error properties	Same as v9.2
7.2.7	**Break detection and correction (Collocating model data)**	Both model and SM data on 0.25° grid.	Model data on 0.25° grid, SM data on 0.1° grid. Nearest neighboring coordinates between grids' points for collocation.

4.1.1 VOD masking

Vegetation influences microwave emission and scattering, and under dense canopies radiation from soil can be completely masked by the vegetation, thus leading to low-quality retrievals. In the MR product, a mask for high VOD is set with a threshold of 0.85 for non-L-band sensors and 0.8 for L-band sensors. Thus, any SSM observation which has a corresponding VOD retrieved larger than the threshold, are filtered out. Threshold values were raised from sensor-frequency specific settings ranging from ~0.5-0.7, as used in the v9.2

main CCI product. Raising VOD thresholds from the ones used in v9.2 avoided over flagging SM values and allowed for sufficient data to propagate into the merging process

4.1.2 Frozen soil masking

Under frozen surface conditions the dielectric properties of the water changes dramatically. Soil is classified as frozen by means of a decision tree based on vertical brightness temperatures at 18.7, 23.8 and 36.5 GHz (van der Vliet, et al., 2020). In the MR product, frozen soil masks were updated with a stricter criterion to exclude frozen soils. There may be several sensors providing observations over a certain grid point on a certain timestamp. In the main CCI v9.2, if any available sensors provided a frozen observation, all other sensors were cross flagged. This approach proved too strict, resulting in excessive data loss. In the MR product, the criterion was changed to require the majority of sensors reporting a frozen flag, to cross-flag all other sensors. These changes allow for sufficient data to propagate throughout the whole merging process, otherwise SM observations would have been drastically over flagged.

4.1.3 Scaling

To correct for seasonal variations in sensor biases, a cumulative distribution function matching is used to calibrate to common climatologies. This method uses a piecewise linear regression between equal sized percentile bins (Liu Y. D., 2012; Liu Y. P., 2011; Moesinger, 2020; Drusch, 2005; Reichle, 2004). CDF-matching is applied for each grid point individually and based on piece-wise linear matching. ACTIVE sensors have been rescaled to ASCAT-B, PASSIVE data to AMSR-E (with the exception to SMAP, which was scaled to AMSR-2), while the COMBINED product all passive and active level 2 data sets are rescaled against GLDASv2.1. For an exhaustive description for the CDF scaling, readers are referred to Section 7.2.3 in the ATBD of CCI v8.1, which is the last CCI product using the CDF scaling methodology (Dorigo W. P.-F., 2023).

In the main v9.2 CCI product, intra-annual scaling to a common climatology was applied to correct for seasonal variations in sensor biases. However, this method proved too computationally extensive for the higher spatial resolution, with no real observed improvements.

4.1.4 Collocating model data

To conserve its integrity, and to stay within reasonable memory and computational limits, model data (ERA5, GLDAS) were not resampled to the 0.1° grid. To collocate satellite-based soil moisture with coordinates on the 0.1° grid, a *k-d tree* based nearest neighbour search was used to find the closest coordinate on the model data's 0.25° grid.

4.2 Resampling

The key difference between the MR product and the main CCI product lies in the grid resolution used to resample the passive radiometer brightness temperature (BT) data and active SM data. The spatial resolution of the MR grid is 0.1° degrees both in longitude and latitude extension, with dimensions of 3600 by 1800 respectively.

For passive BTs, Level-1 swath observations are resampled to a fixed 0.1° grid using the nearest neighbour method, where each output pixel takes the value of the geographically closest input pixel. This is implemented by a *k-d tree* search. This structure is built from the input geolocations and enables efficient lookup of the nearest input pixel index. With these indices, an output array matching the target geometry can be generated using a simple array indexing operation, which is typically very fast. The algorithm uses a 17,500m radius to search for neighbours. If a pixel is found within this radius, the nearest one is chosen; if not, the pixel "Not-a-Number" value is left unassigned (i.e. filled with NaN) (Pyresample, 2025).

Exceptions to this resampling strategy are SMOS and SMAP. The L3 input data for these sensors is provided on the EASEv2 grid (25km and 36km resolution respectively). To transform to the CCI 0.1° grid, the input data is reprojected via GDAL´s *Warp* function, also using nearest neighbour resampling.

Active SSM from H-SAF is provided on a spherical grid constructed using a spiral pattern, where the longitudinal spacing between successive points follows the Fibonacci golden angle (H-SAF, 2024). A two-dimensional Hamming window function centred on each grid node is applied for resampling from the Fibonacci grid to the regular 0.1° grid. This cosine-based weighting function reduces the influence of observations with increasing distance. The window width (25000m) defines which observations contribute to the weighted result, while those outside the window are ignored (H-SAF, 2024). The nature of different resampling methods originates from the fact that ASCAT SSM was provided on a discrete global grid in previous versions to H121 - ASCAT SSM CDR v8, which is used in the MR product. The Hamming window method rectified the differences between the discrete and targeted regular global grid. Future versions of the MR product will explore the synthesisation of resampling algorithms.

Ancillary datasets such as bulk density, clay, sand content and global land cover classification were resampled with the same nearest neighbour method, as used for passive BTs. These datasets are required to compute input parameters (porosity and wilting point) for the Wang and Schmugge model used in LPRM (see (Dorigo W. s.-F., 2024), section 6.1.1).

L-band ancillary data (SMOS CDF matching parameters (see section 6.1.4 of the ATBD v9.0), temperature calibration parameters) are resampled to 0.1° resolution. The SMOS CDF matching parameters are used to fuse the retrieved SM from the different incidence angles of SMOS into one joint SM observation. Ka-band temperatures are needed to obtain surface temperature as input for LPRM. As SMOS does not feature Ka-band, observations of other sensors are used instead. The sensors' Ka-band temperatures are calibrated to AMSR-2 via the aforementioned temperature calibration parameters. The nearest-neighbour resampling is performed such that pixels identified as corresponding to the land mask of the 0.1° product but congruent with a pixel outside of the 0.25° land mask are assigned a valid nearest neighbour from the set of land pixels, with a maximum distance of 20km.

4.3 SSM retrieval

4.3.1 LPRM for radiometer retrievals

Similarly to the main CCI product, the Land Parameter Retrieval Model (LPRM) was utilized to retrieve SM from passive observations. LPRM can simultaneously retrieve SM and vegetation optical depth (VOD) at nadir, using the Microwave Polarization Difference Index (MPDI) calculated from horizontal and vertical polarized BTs. This method is suitable for global mapping, as it is independent of land cover. LPRM is based on a radiative transfer equation (Mo, 1982), which parametrizes the at-sensor radiance as a function of radiation from a vegetation, transmissivity of vegetation (Γv) , the single scattering albedo (ω), the rough surface emissivity (er) and temperatures of soil and vegetation ($Teff, Tc$). This relationship is defined as:

$$TBs(P) = er(P)Teff\Gamma v + (1-\omega)Tc(1-\Gamma v) + (1-er(P))(1-\omega)Tc(1-\Gamma v)\,\Gamma v \quad \textit{Eq. 1}$$

where (P) is the polarization, which is either horizontal or vertical.

In LPRM v6.1 $Teff$ is calculated by a linear regression defined by *(Holmes, 2009)* and shown in *Eq.2*. However, in v7 $Teff$ is obtained via the relationship between Ka-band BT and the average of the ERA5-Land land surface temperature (0 cm) and ERA5-Land layer 1 soil temperature (0–7 cm), with a spatially varying bias term that maximizes the agreement between SM from AMSR2 and SMAP. A spatially varying single scattering albedo (ω) is also used in v7. In the MR product, LPRM v6.1 was used across all radiometers, due to the poor VOD retrieval (especially in dense vegetation) encountered in v7, its complexity and parametrization on reanalysis data.

Thus, LPRM v6.1 was used with its parameters defined in Table 3. These include ω, soil roughness (h), polarization mixing factor (Q), which are key components for calculating $er(P)$ (Wang, 1981)

Table 3: LPRM v6.1 parametrization for various frequencies

Parameter	L-band	C-band	X-band
ω	0.12	0.075	0.075
h	h_1 = 1.1	h_1 = 1.2	h_1 = 1.2
Q	0	0.115	0.127

An important parameter for solving underlying radiative transfer equations in LPRM, are the surface temperatures ($Teff, Tc$) (Holmes, 2009). For all sensors but SMOS and SMAP, vertically polarized Ka-band (37 GHz) BTs, simultaneously taken by the same sensor, were used to retrieve surface T, as shown on *Eq. 2* :

$$Teff = Tc = (0.893\ KaBT) + 44.8 \qquad \textit{Eq. 2}$$

For the L-band (SMAP, SMOS) a temporally matched surface T was used from other sensors. Sources for BTs used for L-band observations are AMSR2, AMSR-E, FY-D, FY-B, GMI, TMI. Observations of these sensors congruent with L-band measurements are utilized under the condition of a maximum time difference of 12h. In case of no corresponding observations are found, no SM can be retrieved for the day with L-band data.

Disentangling the vegetation and soil roughness influences during SM retrieval is difficult (Njoku, 2006). In LPRM the roughness parametrization is updated by a previous VOD calculation to account for vegetation (van Der Schalie R. d.-F.-Y., 2017). However, to produce the MR product, vegetation correction was not applied, because of the excessive overestimation of SM at latitudes higher than 60°. For an exhaustive description of the LPRM algorithm, readers are referred to (De Jeu, 2003), (Meesters, 2005) and (Dorigo W. s.-F., 2024).

4.3.2 H-SAF active datasets

SM from active sensors is provided by H-SAF. The SM retrieval from active sensors is a data-driven change detection algorithm based on C-band backscatter observations. Backscatter data from multiple incidence angles are collected by the algorithm to model both SM and vegetation dynamics. Historical backscatter data time series data provides semi-empirical model parameters, that are needed for surface layer (<5cm) soil water content estimation (H-

SAF, 2024) (Dorigo W. s.-F., 2024). The active SM product used in the COMBINED MR product is H121 - ASCAT SSM CDR v8 12.5 km (Metop ASCAT Surface Soil Moisture Climate Data Record v8 12.5 km sampling).

4.4 RFI

Passive emissions are affected by artificial sources on the ground, the so-called radio frequency interference (RFI). Adequately detecting frequency-dependent RFI allows for LPRM to switch for higher frequencies if affected. RFI calculation builds upon the standard error values that are computed from the correlation coefficients between the time series of two distinct frequency channels and the standard deviation of the time series for the frequency of interest (de Nijs, 2015). As opposed to more traditional approaches, such as the spectral difference method (Li, 2004), this standard error method is more sensitive to weak RFI signals, and it is less prone to producing false positives. In the MR product RFI is calculated for all sensors, except for SMOS and SMAP, for which the input data provides RFI information

5 Dataset characteristics

Below examples visualize the difference between the ESA CCI v9.2 (0.25°) product and the MR product. Islands and peninsulas are better captured by the increased resolution due to the higher resolution land mask. Differences in soil moisture between the products may arise due to differences in LPRM versions used in v9.2 and the MR product, vegetation correction used in LPRM throughout v9.2, changed VOD thresholds, frozen masks and different scaling methodologies.

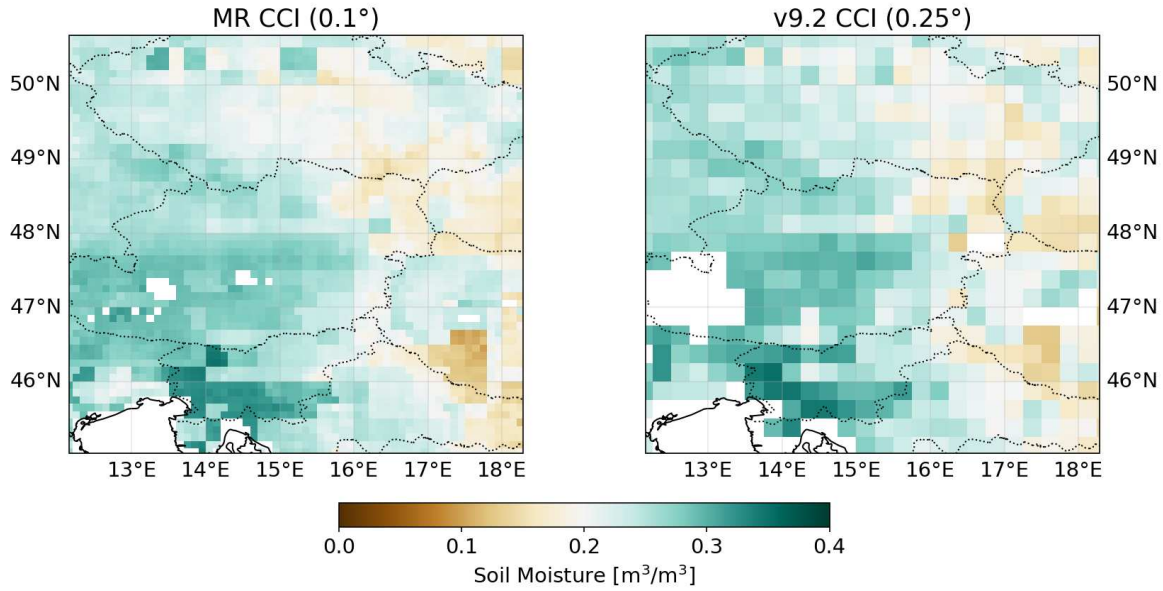

Figure 2: Comparison of spatial characteristics over Central Europe on 2015 5th of June. MR product at 0.1° resolution (left), main v9.2 CCI product at 0.25° resolution (right)

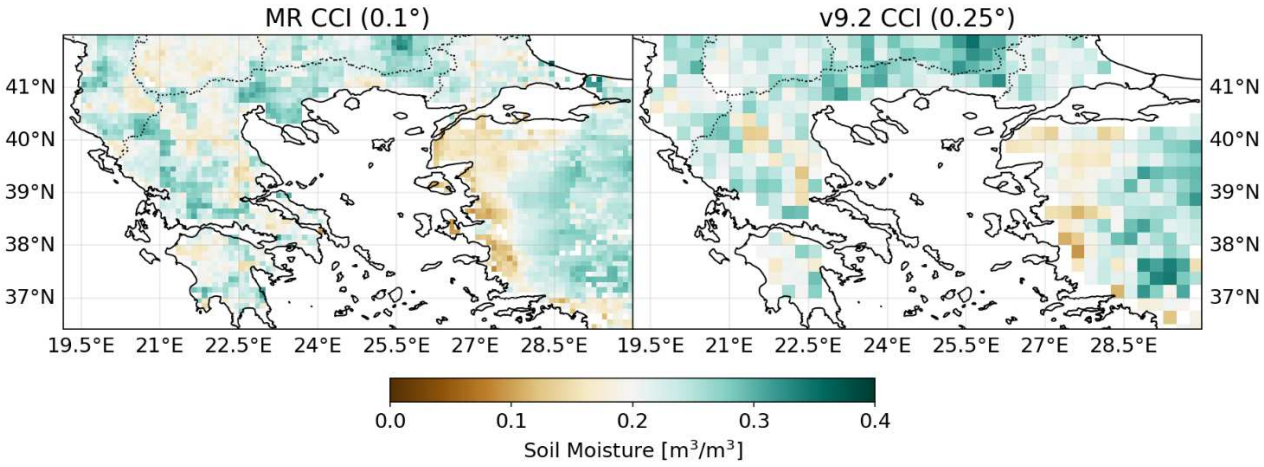

Figure 3: Comparison of spatial characteristics over Greece and Turkey on 2015 5th of June. MR product at 0.1° resolution (left), main v9.2 CCI product at 0.25° resolution (right).

6 Known limitations

- Due to low dynamic range of SM values over desert areas, the break adjustment leads to unreliable results. As a result, these areas are masked in the MR v1.0 product. The inclusion of these areas is planned for the next release.

- Resampling of passive brightness temperatures on coastlines occasionally provided erroneous values, that could result in poor quality SM retrievals.

- Collocation of model data during break detection. Model data was not resampled to match the MR grid, which could lead to lower quality SM data.

7 Appendix

The following section contains preliminary validation results. Final validation is provided as part of the D4.9 Evaluation Report. All validations have been performed using the QA4SM platform.

7.1 Validation against in-situ observations

The MR product was validated to in-situ observations from the International Soil Moisture Network (Dorigo W. H., 2021). The validation against the spatially discrete in-situ observations data requires the ISMN dataset to be chosen as spatial reference. The MR product is used as the temporal reference.

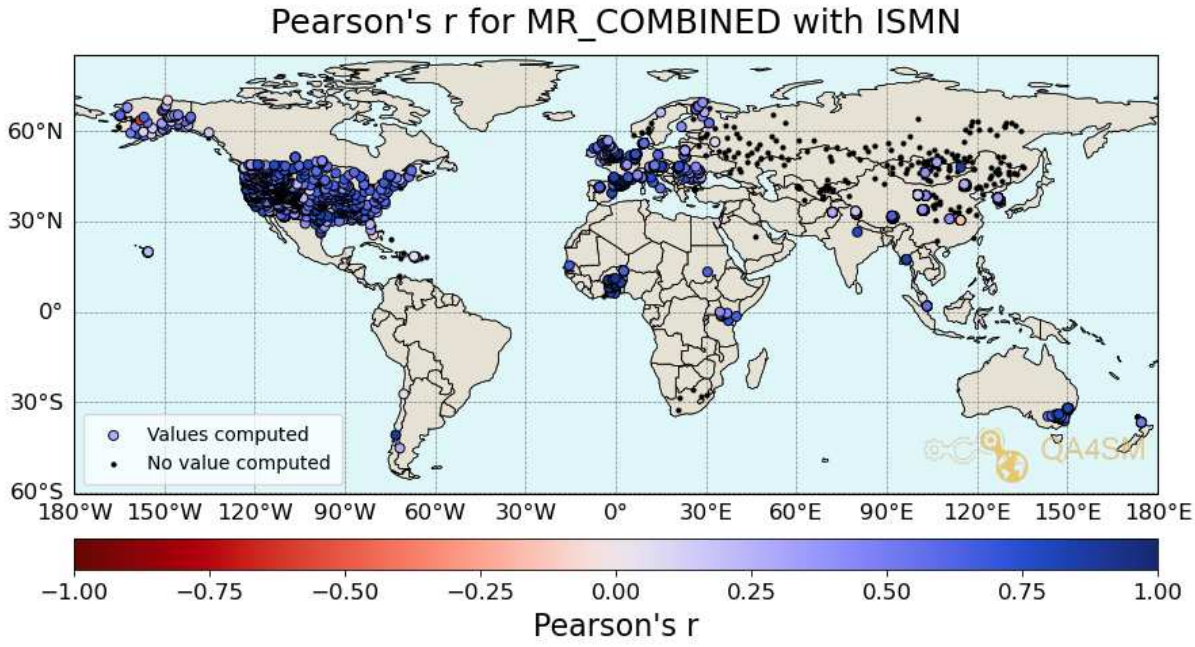

Figure 4: Pearson correlation of the ESA CCI MR product with ISMN stations

Table 4: Correlation statistics - MR product correlated against ISMN

Metric	Mean	Median	IQ range
# observations	1073	607	1549
Pearson's r	0.48	0.53	0.34
Spearman's ρ	0.48	0.53	0.36
Root-mean-square deviation in m^3/m^3	0.1	0.092	0.052
Bias (difference of means) in m^3/m^3	0.001	-0.0058	0.11
Unbiased root-mean-square deviation in m^3/m^3	0.061	0.058	0.033
Mean square error in $(m^3/m^3)^2$	0.012	0.0084	0.01
Mean square error correlation in $(m^3/m^3)^2$	0.0025	0.002	0.0019
Mean square error bias in $(m^3/m^3)^2$	0.0081	0.0032	0.01
Mean square error variance in $(m^3/m^3)^2$	0.0018	0.0011	0.0024
Residual sum of squares in $(m^3/m^3)^2$	13.7	7.2	14.2

7.2 Correlation against reanalysis data

The MR product was compared to reanalysis data, namely the volumetric soil water layer 1 (swvl1) variable, extending from the surface to a depth of 7cm, from the ERA5-Land dataset. The correlation is performed with the MR product as temporal and spatial reference. Agreement is generally high, with lower correlations over densely vegetated areas. Areas of tropical rainforest and desert are masked due to limitations of the SM retrieval algorithm within the MR product.

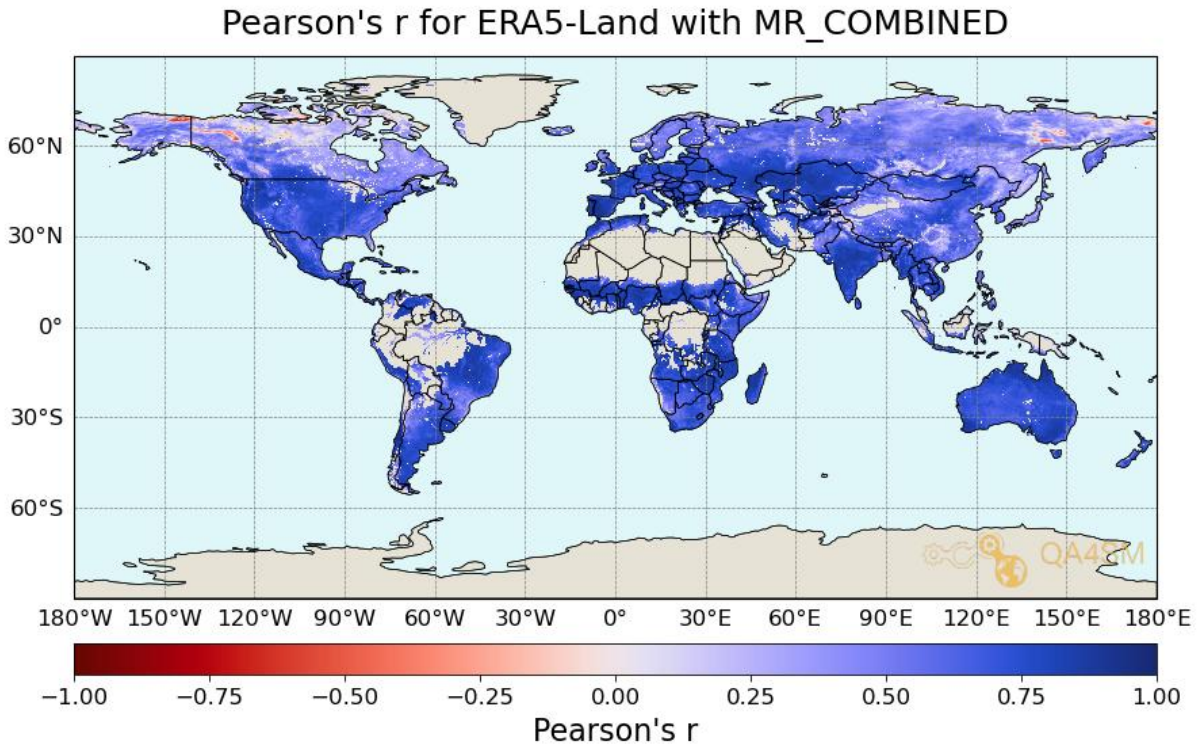

Figure 5: Pearson correlation of the ESA CCI MR product with ERA5-Land (swvl1)

Table 5: Correlation statistics - MR product correlated against ERA5-LAND (swvl1)

Metric	Mean	Median	IQ range
# observations	3877	3618	5725
Pearson's r	0.57	0.62	0.3
Spearman's ρ	0.57	0.62	0.3
Root-mean-square deviation in m^3/m^3	0.1	0.091	0.052
Bias (difference of means) in m^3/m^3	-0.055	-0.055	0.1
Unbiased root-mean-square deviation in m^3/m^3	0.054	0.051	0.02
Mean square error in $(m^3/m^3)^2$	0.015	0.0083	0.0098
Mean square error correlation in $(m^3/m^3)^2$	0.0022	0.0019	0.0014
Mean square error bias in $(m^3/m^3)^2$	0.012	0.0049	0.01
Mean square error variance in $(m^3/m^3)^2$	0.00099	0.00069	0.001
Residual sum of squares in $(m^3/m^3)^2$	62.5	38.5	41.5

7.3 Correlation against ESA CCI SM v9.2 COMBINED (coarse resolution)

The MR product serves as the spatial reference for the validation against the main ESA CCI product. As temporal reference, ESA CCI v9.2 COMBINED is arbitrarily chosen as both datasets share equal timesteps. The agreement of the MR product is generally high when compared to v9.2 COMBINED, with lower correlations in higher latitudes i.e.: Siberia, North Canada. This could be mainly explained by the difference in retrieval algorithms, particularly the absence of vegetation correction in LPRM used in the MR product, as well as different scaling methodologies.

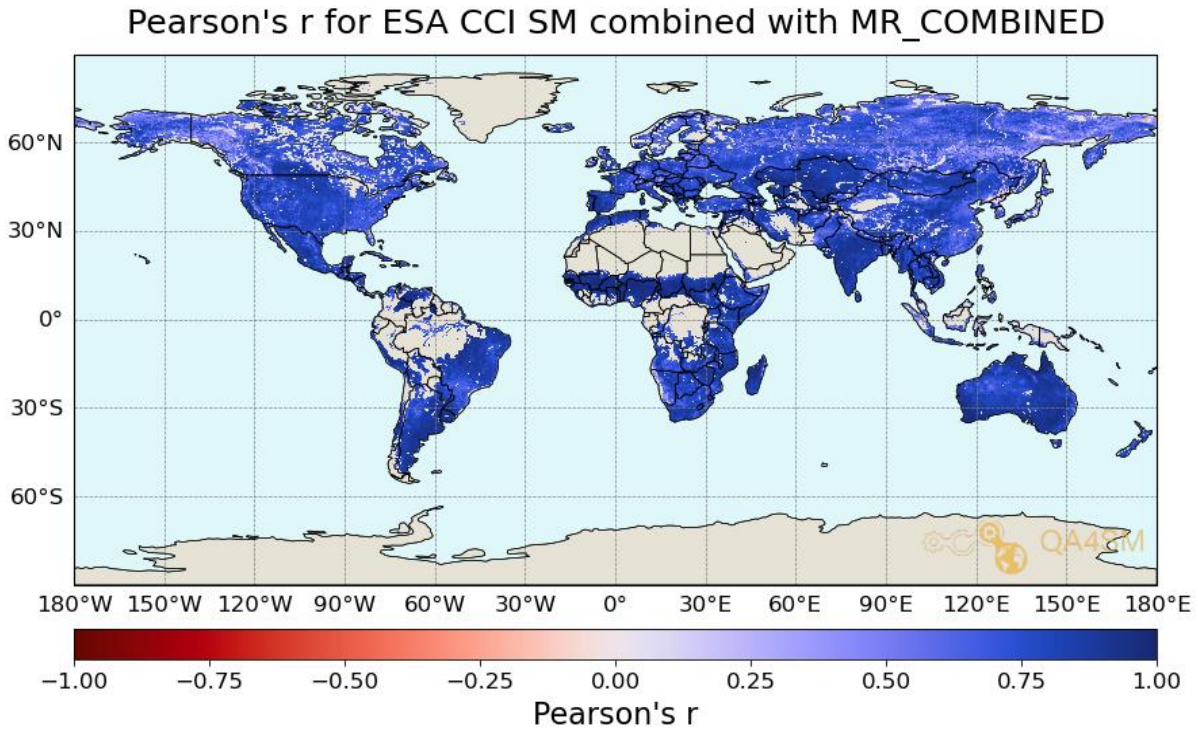

Figure 6: Pearson correlation of the ESA CCI Medium Resolution product with ESA CCI v9.2 COMBINED

Table 6: Correlation statistics - MR product correlated against ESA CCI v9.2 COMBINED

Metric	Mean	Median	IQ range
# observations	3270	2749	6046
Pearson's r	0.72	0.75	0.18
Spearman's ρ	0.72	0.75	0.18
Root-mean-square deviation in m^3/m^3	0.031	0.029	0.012
Bias (difference of means) in m^3/m^3	0.0023	0.0023	0.011
Unbiased root-mean-square deviation in m^3/m^3	0.029	0.028	0.011
Mean square error in $(m^3/m^3)^2$	0.001	0.00086	0.00072
Mean square error correlation in $(m^3/m^3)^2$	0.00089	0.00074	0.00062
Mean square error bias in $(m^3/m^3)^2$	0.00011	3.4e-05	0.0001
Mean square error variance in $(m^3/m^3)^2$	3.5e-05	1.1e-05	3.2e-05
Residual sum of squares in $(m^3/m^3)^2$	5.03	3.16	5.28

8 Bibliography

Chug, D. D. (2023). Dry-to-Wet Soil Gradients Enhance Convection and Rainfall over Subtropical South America. *Journal of Hydrometeorology*.

De Jeu, R. A. (2003). Further validation of a new methodology for surface moisture and vegetation optical depth retrieval . *International Journal of Remote Sensing*.

de Nijs, A. P. (2015). A methodology to determine radio-frequency interference in AMSR2 observations. *IEEE Transactions on Geoscience and Remote Sensing,*.

Dorigo, W. H. (2021). The International Soil Moisture Network: serving Earth system science for over a decade. *Hydrology and Earth System Sciences Discussions*, pp.1-83.

Dorigo, W. P.-F. (2023). ESA Climate Change Initiative Plus - Soil Moisture Algorithm Theoretical Baseline Document (ATBD) Supporting Product Version 08.1 (version 1.1). *Zenodo*.

Dorigo, W. s.-F. (2024). ESA Climate Change Initiative Plus - Soil Moisture Algorithm Theoretical Baseline Document (ATBD) Supporting Product Version 09.0. *Zenodo*.

Drusch, M. W. (2005). Observation operators for the direct assimilation of. *e. Geophysical Research Letters*.

Holmes, T. D. (2009). Land surface temperature from Ka band (37 GHz) passive microwave observations. *Journal of Geophysical Research: Atmospheres*.

H-SAF. (2024). Algorithm Theoretical Baseline Document (ATBD) Metop ASCAT Surface Soil Moisture Near Real Time 6.25 km sampling (H122). *v0.1*.

Li, L. N. (2004). A preliminary survey of radio-frequency interference over the US in Aqua AMSR-E data. *IEEE Transactions on Geoscience and Remote Sensing*.

Liu, Y. D. (2012). Trend-preserving blending of passive and active microwave soil. *Remote Sensing of Environment*.

Liu, Y. P. (2011). Developing an improved soil moisture dataset by blending passive and. *Hydrology and Earth System Sciences*.

Mathon, V. L. (2002). Mesoscale convective system rainfall in the Sahel. *Journal of Applied Meteorology and Climatology*, 41(11), 1081–1092.

Meesters, A. D. (2005). Analytical derivation of the vegetation optical depth from the microwave polarization difference index. *IEEE Geoscience and Remote Sensing Letters,*.

Mo, T. C. (1982). A model for microwave emission from vegetation-covered fields. *ournal of Geophysical Research: Oceans*.

Moesinger, L. a. (2020). The global long-term microwave Vegetation Optical Depth. *Earth System Science Data*.

Njoku, E. a. (2006). Vegetation and surface roughness effects on AMSR-E land observations. *Remote Sensing of environment*.

Pyresample. (2025). *https://pyresample.readthedocs.io/en/latest/index.html*.

Reichle, R. K. (2004). Global Soil Moisture from Satellite. *Journal Of Hydrometeorology*.

Taylor, C. M. (2011). Frequency of Sahelian storm initiation enhanced over mesoscale soil-moisture patterns. *Nature Geoscience*, 4(7), 430–433.

van Der Schalie, R. d.-F.-Y. (2017). The merging of radiative transfer based surface soil moisture data from SMOS and AMSR-E. *Remote Sensing of Environment*.

van Der Schalie, R. K.-F.-Y. (2016). Global SMOS soil moisture retrievals from the land parameter retrieval model. *International journal of applied earth observation and geoinformation*.

van der Vliet, M., van der Schalie, R., Rodriguez-Fernandez, N., Colliander, A., Jeu, R. d., Preimesberger, W., . . . Dorigo, W. (2020). Reconciling Flagging Strategies for Multi-Sensor Satellite Soil Moisture Climate Data Records. doi:10.3390/rs12203439

Wang, J. a. (1981). Remote sensing of soil moisture content, over bare field at 1.4 GHz frequency. *Journal of Geophysical Research: Oceans*.